Fibers and Polymers 2017, Vol.18, No.3, 549-554
DOI 10.1007/s12221-017-6399-1

ISSN 1229-9197 (print version)
ISSN 1875-0052 (electronic version)

Structural Difference of Gel-spun Ultra-high Molecular Weight Polyethylene Fibers Affected by Cold Drawing Process

Minfang An, Haojun Xu, You Lv, Qun Gu[1], and Zongbao Wang*

Ningbo Key Laboratory of Specialty Polymers, Faculty of Materials Science and Chemical Engineering, Ningbo University, Ningbo 315211, China
[1]*College of Material Engineering, Ningbo University of Technology, Ningbo 315211, China*
(Received April 6, 2016; Revised October 24, 2016; Accepted November 21, 2016)

Abstract: The UHMWPE fibers with different cold drawing ratio (DR_0) were obtained from the industrial UHMWPE fibers production line. The effect of cold drawing before the extraction of paraffin oil process on final fibers was investigated by tensile testing, small angle X-ray scattering (SAXS) and wide angle X-ray diffraction (WAXD). The tensile strength and modulus with 5.0 DR_0 were 2.99 and 151.5 GPa, respectively, which were 13.3 % and 41.9 % higher than those with 1.5 DR_0. With the increase of DR_0, the values of average shish length decreased obviously, while the shish orientation increased and the apparent crystal size along two lattice directions ($(110)_o$ and $(200)_o$) in UHMWPE fibers decreased. The increase of degree of orientation and crystallization were verified that better folded chains and amorphous chains were involved in forming shorter and better oriented shish.

Keywords: UHMWPE fibers, Cold drawing, Shish structure, Orientation, Crystallization

Introduction

Ultra-high molecular weight polyethylene (UHMWPE) fibers produced by gel-spinning method have distinctive properties such as high strength, high modulus, high wear and cutting resistance [1-3]. The superior mechanical properties of UHMWPE fibers are mainly ascribed to the highly oriented and fully extended chains in the highly crystalline structure [4,5]. Litvinov *et al.* [6] revealed the structural and morphological changes at the final stage of the fiber drawing process and they thought that the stretching caused the increase of crystallinity and chain orientation. The hot drawing process in the preparation of UHMWPE fibers can generate the strong flow field and induce the formation of shish-kebab crystals [7,8]. The shish-kebab developed in both the as-spun and drawn fibers can be transformed continuously into the micro-fibril structure composed mostly of the shish structure through the hot drawing process [9].

Until now, related studies have placed almost all of their focus on the ultimate mechanical properties and mechanism of structural development of the hot drawing process with UHMEPE fibers [10-13]. Little attention has been paid to the effect of cold drawing before the extraction of paraffin oil process and structural difference of gel-spun UHMWPE fibers with high concentration spinning solution and speed spinning process after cold drawing. Therefore, in this study, the samples were obtained with different cold drawing ratio from the industrial UHMWPE fiber production line, and the mechanical performance, parameters of shish, degree of orientation and crystallization were measured.

*Corresponding author: wangzongbao@nbu.edu.cn

Experimental

Materials

The UHMWPE resin used in this study is associated with a viscosity-average molecular weight ($\overline{M}_V$) of 3.5×10^6, which was supplied by Sinopec Beijing Yanshan Company.

Sample Preparation

The UHMWPE gels were prepared by twin-screw extruder at 150-250 °C with 8 wt% UHMWPE solutions in paraffin oil. The hot homogenized gels were then gel-spinning using spinneret plate with 240 conical dies with an exit diameter of 1 mm at an extrusion rate of 8 m/min and an extrusion temperature of 248 °C. After spinning from the spinneret, the fibers were cold drawn to different drawing ratios (DR_0) at room temperature. The gel-spinning fibers were then extracted in a dichloromethane bath to remove paraffin oil. Finally, fibers were gone through three hot-drawing stages at the temperature of 110, 120 and 130 °C, respectively. The details are listed in Table 1. The total hot-drawing ratio (THDR) and total drawing ratio (TDR) are respectively defined as follows:

$$THDR = DR_1 \times DR_2 \times DR_3 \quad (1)$$

Table 1. Samples identification and the draw ratio of cold drawing and hot drawing of UHMWPE fibers

Sample	DR_0	DR_1	DR_2	DR_3	THDR	TDR
C1	1.5	5.5	2.5	1.5	20.6	30.9
C2	4.0	4.0	2.1	1.4	11.8	47.0
C3	5.0	3.7	2.0	1.4	10.3	51.8

$$TDR = DR_0 \times DR_1 \times DR_2 \times DR_3 \quad (2)$$

where DR_0, DR_1, DR_2 and DR_3 are the draw ratio of cold drawing, first hot-drawing stage, second hot-drawing stage and third hot-drawing stage, respectively.

Tensile Test

Tensile test of UHMWPE fibers with no twisting was performed on an Instron 5567 tension testing machine at a tensile rate of 250 mm/min, and the fiber initial gauge length was 500 mm.

The SAXS and WAXD Measurement

The wide-angle X-ray diffraction (WAXD) and small-angle X-ray scattering (SAXS) measurements were carried out at the BL16B1 beamline in the Shanghai Synchrotron Radiation Facility (SSRF). The wavelength of the synchrotron radiation was 0.124 nm. Two-dimensional (2D) WAXD and SAXS patterns were collected by using a Mar CCD X-ray detector (MAR165), having a resolution of 2048×2048 pixels. The beam intensity monitor before sample was a N_2 gas ionization chamber, and the monitor after sample adsorption was a photodiode in the beam stop. Two scatter-less slits (Xenocs) were used to depress parasitic scattering. The sample holder was mounted onto an optical table [14]. The sample-to-detector distance was 5139 mm for SAXS and 188 mm for WAXD. The SAXS and WAXD image acquisition time of each data frame was 5 s and 2 s, respectively. All X-ray images were corrected for background scattering, air scattering, and beam fluctuations. The WAXD and SAXS measurement date analysis were carried out by the Fit2d software package [15].

Table 2. The mechanical properties of UHMWPE fibers with different DR_0

Sample	Fineness (dtex)	Tensile strength (GPa)	Modulus (GPa)	Ultimate elongation (%)
C1	2.84	2.64±0.09	106.8±4.5	3.29±0.13
C2	1.84	2.90±0.14	140.3±5.1	2.85±0.11
C3	1.58	2.99±0.13	151.5±6.1	2.69±0.07

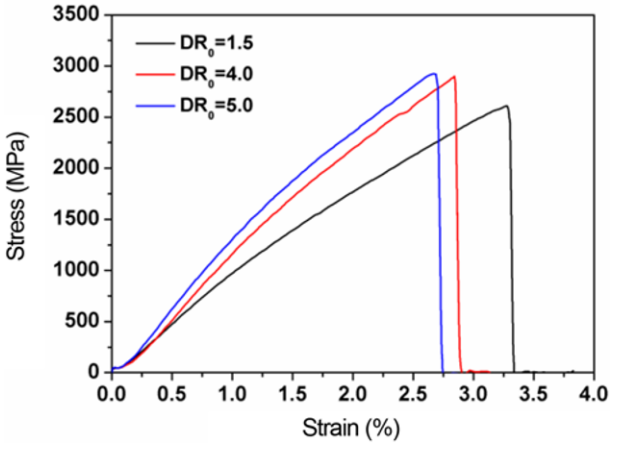

Figure 1. The stress-strain curves for UHMWPE fibers with different DR_0 at the rate of 250 mm min^{-1}.

Results and Discussion

Table 2 shows the mechanical properties of the UHMWPE fibers with different cold drawing ratios. The fineness of UHMWPE fibers is decreased with the increase of DR_0 because of the increase of the total drawing ratio (TDR) listed in Table 1. With the increase of DR_0, the total hot-drawing ratio (THDR) decreases though TDR are increased (Table 1). Figure 1 shows the stress-strain curves for UHMWPE fibers with different DR_0. The increase of DR_0 significantly enhances the ultimate tensile strength and Young's modulus of UHMWPE fibers, although the THDR obviously decreases. Compared with UHMWPE fibers with 1.5 DR_0, the ultimate tensile strength and Young's modulus of UHMWPE fibers are improved by about 9.8 % and 31.4 %, respectively, with the DR_0 increased to 4.0. Moreover, with the DR_0 of 5.0, the ultimate tensile strength and Young's modulus of UHMWPE fibers are improved by 13.3 % and 41.9 %, respectively. These results indicate that the process of cold drawing has a significantly influence on the mechanical properties of UHMWPE fibers.

The 2D WAXD patterns of UHMWPE fibers with different DR_0 are shown in Figure 2. All 2D WAXD patterns show

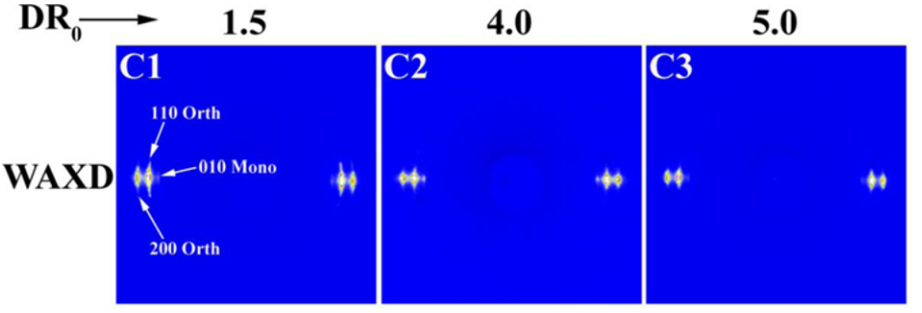

Figure 2. 2D WAXD patterns of UHMWPE fibers with different DR_0.

$(110)_{Orth}$, $(200)_{Orth}$ reflections of orthorhombic unit cell and $(010)_{Mono}$ reflection of monoclinic unit cell. The 2D WAXD pattern of UHMWPE fibers with 1.5 DR_0 shows the broaden diffraction reflections implied the imperfect lamellar crystallite orientations. And with the increase of DR_0, the diffraction reflections of $(110)_{Orth}$, $(200)_{Orth}$ and $(010)_{Mono}$ become more narrow. These indicate that the lamellar crystallite orientations become more perfect with the increase of DR_0, although THDR is decreased. It implies that the cold drawing process has an important influence on the microcrystalline structure of UHMWPE fibers.

In order to further investigate the influence of cold drawing on the structure of UHMWPE fibers, more detailed information from the 2D WAXD patterns are obtained. Apparent crystal size (L_{hkl}) of UHMWPE fibers could be computed using by Scherrer's equation [16]:

$$L_{hkl} = \frac{k\lambda}{\beta\cos\theta_{hkl}} \tag{3}$$

where λ is the X-ray wavelength, k is a dimensionless shape factor, β is the half width of the (hkl) reflection at a scattering angle 2θ, θ is the Bragg angle.

2D WAXD patterns (Figure 2) were analyzed to calculate the degree of crystallinity, X_c, of UHMWPE fibers with different DR_0 from equation (4).

$$X_c = \frac{\int_0^\infty s^2 I_c(s)ds}{\int_0^\infty s^2 I_t(s)ds} \qquad I_t(s) = I_c(s) + I_a(s) \tag{4}$$

where s is the scattering vector ($s=2\sin\theta/\lambda$), $I_c(s)$ and $I_a(s)$ represent the integrated diffraction intensity of the crystal phase (Figure 3) and the scattered intensity of the amorphous phase at s, respectively. It is the integrated diffraction intensity (azimuthal angle, Ø=0-360 °) due to the sum of amorphous and crystal phases. The WAXD profile was curve-fitted by applying Voight functions.

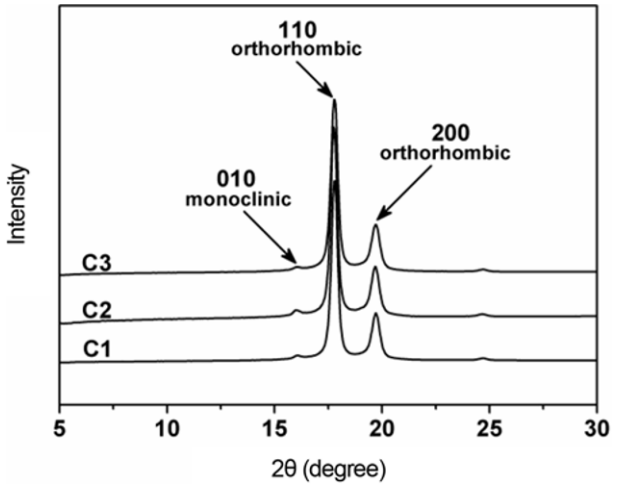

Figure 3. 1D WAXD intensity profiles of UHMWPE fibers with different DR_0.

Quantitatively, the degree of crystal orientation in UHMWPE fibers with different DR_0 was determined by using the Herman's method [16]. Accordingly, the crystalline orientation can be characterized by average orientation of the normal to the crystalline plane with respect to an external reference frame. Here, the fiber axis direction was taken as the reference direction. For a set of *hkl* planes, the average orientation, expressed as $\langle\cos^2\text{Ø}\rangle_{hkl}$, can be calculated mathematically using the following equation:

$$\langle\cos^2\text{Ø}\rangle_{hkl} = \frac{\int_0^{\pi/2} I(\text{Ø})\cos^2\text{Ø}\sin\text{Ø}d\text{Ø}}{\int_0^{\pi/2} I(\text{Ø})\sin\text{Ø}d\text{Ø}} \tag{5}$$

where Ø is the azimuthal angle and I(Ø) is the scattered intensity along the angle Ø. Herman's orientation function, f, is defined as

$$f = \frac{3\langle\cos^2\text{Ø}\rangle_{hkl} - 1}{2} \tag{6}$$

where f has the value of -0.5, when the normal of the reflection plane is perpendicular to the reference direction (Ø=90 ° or crystals are oriented parallel to the fiber axial direction), a value of 1, when the normal is parallel to the reference direction (Ø=0 ° or crystals are oriented perpendicularly to the fiber axial direction), and a value of 0, when the orientation is random. The degree of orientation, f_{110}, are calculated from the azimuthal intensity distribution, I(Ø), of the (110) reflection, of α-crystals in UHMWPE fibers with different DR_0.

The 1D WAXD intensity profiles of UHMWPE fibers with different DR_0 are shown in Figure 3. Comparing from the intensity and position of diffraction peaks $(010)_m$, $(110)_o$, $(200)_o$, there is no any obvious difference between various fibers intensity profiles. To distinguish their differences, the apparent crystal sizes were calculated and shown in Table 3. The degree of crystallinity and orientation of UHMWPE fibers with different DR_0 are also listed in Table 3. It can be seen that the apparent crystal size along two lattice directions ($(110)_o$ and $(200)_o$) in UHMWPE fibers are decreased with the increase of DR_0, while THDR is decreased. In this study, the highest TDR of UHMWPE fibers is 51.8, which is much lower than that of UHMWPE fibers are completely composed of extended chain crystals. Besides, the 2D SAXS patterns

Table 3. Apparent crystal size (L_{110} and L_{200}), the degree of crystallinity and orientation of UHMWPE fibers with different DR_0

Sample	L_{110} (nm)	L_{200} (nm)	Crystallinity (%)	f_{110}	f_{200}
C1	20.4	15.0	89.42	0.919	0.913
C2	19.6	14.4	91.23	0.927	0.924
C3	18.9	14.3	93.44	0.936	0.939

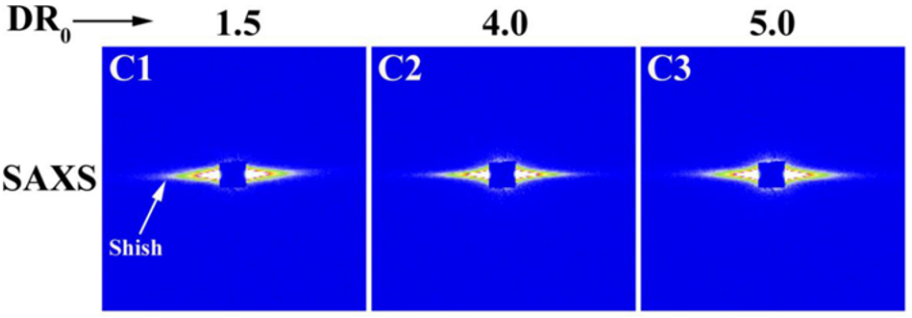

Figure 4. 2D SAXS patterns of UHMWPE fibers with different DR_0.

(Figure 4) show no scattering patterns of lamellar crystal (kebab), which indicates that lamellar crystals transformed to microfibrils at relatively lower draw ratio compared with TDR. So the fibers are constituted by most of microfibrils (imperfect shish crystal) and a small amount of extended chain crystals (perfect shish crystal). The apparent crystal size of UHMWPE fibers decreases with DR_0 increased due to the process of unfolding into extended chain [17]. It indicates that the transformation extent of microfibrils to extended chain crystals improves with the increase of DR_0. The degree of orientation of UHMWPE fibers improves with the increase of DR_0, which also supports that cold drawing process is beneficial for the transformation of microfibrils to extended chain crystals. Moreover, with the increase of DR_0, the degree of crystallization is increased, which indicates that more amorphous chains are involved to form shish crystal. So the ultimate tensile strength and Young's modulus of UHMWPE fibers are improved with the increase of DR_0.

Figure 4 shows the 2D SAXS patterns of UHMWPE fibers with different DR_0. Strong equatorial streaks appear for all samples, as indicated by the arrow in Figure 4. The appearance of the equatorial streak is consistent with the formation of shish (In fact this shish structure is consisted of microfibril and extended chain crystal which have similar structure with shish) having strong electron density contrast with the surrounding matrix which may be related to the multiple shish in the UHMWPE fibers. In this study, the THDR of various samples is decreased instead of equal with DR_0 increased, although TDR is increased. But it can be clearly seen that the equatorial streak of UHMWPE fibers with 5.0 DR_0 is stronger than those with 1.5 DR_0, which implies the high DR_0 fiber has better shish structure.

To better investigate the difference of the shish structure with the different DR_0, the changes of the average shish length, $<L_{shish}>$, and the misorientation of shish, $B_{Ø}$, were followed. These parameters were obtained by using the Ruland streak method to analyze the equatorial streak feature in SAXS [18-20]. Ruland demonstrated that the size and orientation distributions of longitudinal voids in polymer and carbon fibers in real space could be estimated from the equatorial streak of SAXS in reciprocal space (as long as the orientation and the longitudinal length of scatterer are finite). Since the method is principally based on the separation of experimentally measured azimuthal breadth from contributions of scatterer length and misorientation, the method can also be applied to separate the average length of shish and its average misorientation. If one assumes that all azimuthal distributions can be modeled by Lorentz functions, the observed azimuthal width, B_{obs}, can be related to the length of shish, $<L_{shish}>$, and the azimuthal width, $B_{Ø}$, due to misorientation of shish by the following equation.

$$B_{obs} = \frac{1}{<L_{shish}>s} + B_{Ø} \tag{7}$$

If all azimuthal distributions have Gaussian expressions, then the relationship becomes

$$B_{obs}^2 = \left(\frac{1}{<L_{shish}>s}\right)^2 + B_{Ø}^2 \tag{8}$$

where B_{obs} represents the integral width of the azimuthal profile from the equatorial streak at s. On the basis of equation (7) or equation (8), $<L_{shish}>$ can be obtained from

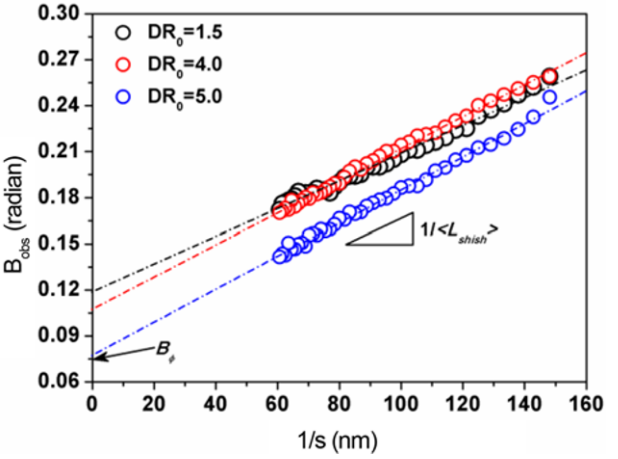

Figure 5. Plot of azimuthal integral width (B_{obs}) vs the value of 1/s, which was used to determine the average shish length ($<L_{shish}>$) and the shish misorientation ($B_{Ø}$) based on equation (7).

Table 4. The average shish length ($<L_{shish}>$) and the shish misorientation ($B_{Ø}$) of UHMWPE fibers with different DR_0

Sample	$<L_{shish}>$ (nm)	$B_{Ø}$ (degree)
C1	1098	6.77
C2	962	6.17
C3	934	4.49

the slope, and the misorientation width, $B_{Ø}$ can be obtained from the intercept of the plots (B_{obs} vs s^{-1} or B^2_{obs} vs s^{-2}). In this study, we found that all azimuthal distributions were better fit with Lorentz functions, thus the plot based on equation (7) (as shown in Figure 5) was used to determine $<L_{shish}>$ and $B_{Ø}$.

The average shish length ($<L_{shish}>$) and the shish misorientation ($B_{Ø}$) of UHMWPE fibers with different DR_0 are shown in Table 4. The average shish length ($<L_{shish}>$) and the shish misorientation ($B_{Ø}$) of UHMWPE fibers are both decreased with the increase of DR_0. These results indicate that the shish structure becomes more perfect with the increase of DR_0, which corresponds to the result of the degree of orientation of UHMWPE fibers. Shorter shish structure leads to the the higher degree of orientation.

In general, in the high concentration of spinning solution, the UHMWPE chains are more entangled, resulting in dense network with more physical cross-linking points. The high entanglement concentration is not good to the transformation of shish-kebab to shish crystal and makes as-spun fibers poor drawability. Reducing the number of entanglements is the key precondition to obtain higher properties UHMWPE fibers, although a minimum number of entanglements are necessary to ensure sufficient coherence of the entanglement network and avoid premature breakage of the spinline [21,22]. Molecular chain entanglement is loose with the solvent, and with the corresponding action force, the gel-network structure will be disentangled. So cold drawing before the extraction of paraffin oil process is beneficial to reduce the number of entanglements and then make molecular orient better and more molecular take part in crystallization, which supports the above result that the degree of crystallization and orientation are both increased with the increase of DR_0. The hot-drawing is the most important process for UHMWPE fibers obtain the high mechanical property, which could make the molecular take part in extended chain crystal. The shish-kebab crystal could be formed when gel-spun UHMWPE fibers were gone through hot-drawing process with low draw ratio [23-25]. And with the increase of hot-drawing ratio, the shish-kebab crystal gradually transformed to extended chain crystal, which makes UHMWPE fibers have excellent properties [24-28]. Cold drawing process reducing the number of entanglements makes more molecular take part in extended chain crystal and accelerates the transformation of shish-kebab crystal to extended chain crystal, which responds that the transformation extent of microfibrils to extended chain crystals improves with the increase of DR_0.

Conclusion

The UHMWPE fibers with different DR_0 were obtained from the industrial UHMWPE fibers production line. The increase of DR_0 significantly enhances the ultimate tensile strength and Young's modulus of UHMWPE fibers, although the THDR obviously decreases. And the apparent crystal size along two lattice directions ($(110)_o$ and $(200)_o$) in UHMWPE fibers are both decreased with the increase of DR_0. When the DR_0 came to 5.0, the shish structure and shish orientation exhibited the best. The increase of degree of orientation and crystallization show that the more folded chains and amorphous chains are involved in forming better oriented shish crystal. The above results suggest that cold drawing process is conducive to the transformation of shish-kebab crystal to extended chain crystal. This research is expected to be helpful for understanding the structural development in industrial production of UHMWPE fibers.

Acknowledgments

This work was supported by the National Science Foundation of China (51273210), Open Research Fund of State Key Laboratory of Polymer Physics and Chemistry, Changchun Institute of Applied Chemistry, Chinese Academy of Sciences and K. C. Wong Magna Fund in Ningbo University. We thank Shanghai Synchrotron Radiation Facility (SSRF) for supporting the WAXD and SAXS tests.

References

1. L. Xia, P. Xi, and B. W. Cheng, *Mater. Lett.*, **147**, 79 (2015).
2. L. Shen, M. Peng, F. Qiao, and J. L. Zhang, *Chin. J. Polym. Sci.*, **26**, 653 (2008).
3. H. J. Xu, M. F. An, Y. Lv, Z. B. Wang, and Q. Gu, *Chin. J. Polym. Sci.*, **34**, 1 (2016).
4. A. Zwijnenburg, P. F. Van Hutten, A. J. Pennings, and H. D. Chanzy, *Colloid Polym. Sci.*, **256**, 729 (1978).
5. Y. L. Hsieh and X. P. Hu, *J. Polym. Sci. Polym. Phys.*, **35**, 623 (1997).
6. V. M. Litvinov, J. J. Xu, C. Melian, D. E. Demco, M. Möller, and J. Simmelink, *Macromolecules*, **44**, 9254 (2011).
7. I. Steyaert, M. P. Delplancke, G. V. Assche, H. Rahier, and K. D. Clerck, *Polymer*, **54**, 6809 (2013).
8. E. L. Heeley, T. Gough, D. J. Hughes, W. Bras, J. Rieger, and A. J. Ryan, *Polymer*, **54**, 6580 (2013).
9. Y. Ohta, H. Murase, and T. J. Hashimoto, *J. Polym. Sci. Polym. Phys.*, **48**, 1861 (2010).
10. M. Xiao, J. Yu, J. Zhu, L. Chen, J. Zhu, and Z. Hu, *J. Mater. Sci.*, **46**, 5690 (2011).

11. B. Kalb and A. J. Pennings, *J. Mater. Sci.*, **15**, 2584 (1980).
12. J. Smook and A. J. Pennings, *J. Appl. Polym. Sci.*, **27**, 2209 (1982).
13. W. Hoogsteen, G. Ten Brinke, and A. J. Pennings, *J. Mater. Sci.*, **25**, 1551 (1990).
14. F. Tian, X. H. Li, Y. Z. Wang, C. M. Yang, P. Zhou, J. Y. Lin, J. R. Zeng, C. X. Hong, W. Q. Hua, X. Y. Li, X. R. Miao, F. G. Bian, and J. Wang, *Nucl. Sci. Tech.*, **26**, 1 (2015).
15. A. P. Hammersley, S. O. Svensson, and A. Thompson, *Nucl. Instrum. Methods Phys. Res., Sect. A,* **346**, 312 (1994).
16. L. E. Alexander, "X-ray Diffraction in Polymer Science", Wiley: New York, 1969.
17. N. A. J. M. Van Aerle, and A. W. M. Braam, *J. Mater. Sci.*, **23**, 4429 (1988).
18. W. Ruland, *J. Polym. Sci. Part C: Polym. Symp.*, **28**, 143 (1969).
19. W. Ruland and R. Perret, *J. Appl. Crystallogr.,* **2**, 209 (1969).
20. W. Ruland and R. Perret, *J. Appl. Crystallogr.,* **3**, 525 (1970).
21. W. O. Statton, *J. Appl. Phys.*, **38**, 4149 (1967).
22. K. Furuhata, T. Yokokawa, C. Seoul, and K. MiyasakaI, *J. Polym. Sci. Polym. Phys.,* **24**, 59 (1986).
23. J. Smook and A. J. Pennings, *J. Appl. Polym. Sci.,* **27**, 2209 (1982).
24. W. Hoogsteen, A. J. Pennings, and G. Tenbrinke, *Colloid Polym. Sci.,* **268**, 245 (1990).
25. A. J. Pennings and J. Smook, *J. Mater. Sci.*, **19**, 3443 (1984).
26. D. Krueger and G. S. Y. Yeh, *J. Polym. Sci. Polym. Phys.*, **6**, 431 (1972).
27. J. T. Yeh, S. C. Lin, C. W. Tu, K. H. Hsie, and F. C. Chang, *J. Mater. Sci.*, **43**, 4892 (2008).
28. V. M. Litvinov, J. J. Xu, C. Melian, D. E. Demco, and M. Moller, *Macromolecules*, **44**, 9254 (2011).